Letter

Radiative Exchange between Graphitic Nanostructures: A Microscopic Perspective

Anh D. Phan,*[†,‡] Sheng Shen,[§] and Lilia M. Woods*[†]

[†]Department of Physics, University of South Florida, Tampa, Florida 33620, United States
[‡]Institute of Physics, Vietnam Academy of Science and Technology, 10 Dao Tan, Ba Dinh, Hanoi 10000, Vietnam
[§]Department of Mechanical Engineering, Carnegie Mellon University, Pittsburgh, Pennsylvania 15213, United States

ABSTRACT: Electromagnetic radiative heat exchange involving graphene nanostrucrures is studied using an atomistic approach based on the coupled dipole method modified by the fluctuation dissipation theorem. This method includes taking into account many-particle electromagnetic contributions and enables treating two or more nanostructures with nontrivial boundary conditions at different temperatures. We present a microscopic picture of the heat exchange process in graphene nanostructured based systems in terms of a transmission coefficient, characteristic temperature function, and atomic morphology. Our studies provide general pathways of near-field radiation control at the nanoscale.
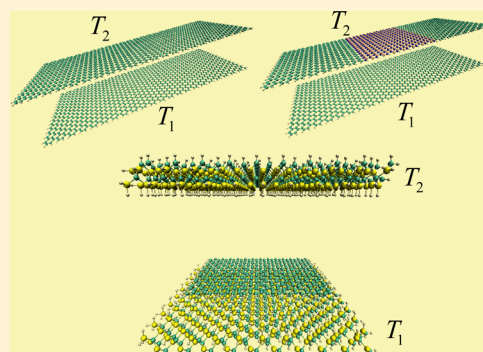
SECTION: Energy Conversion and Storage; Energy and Charge Transport

The energy exchange due to the electromagnetic radiation is a problem of fundamental importance for many physical, chemical, and biological systems. The radiation between objects at small separations is sensitive to their molecular and electronic properties. A great deal of attention has been paid to confined optical fields at the nanoscale. Such fields can be used for novel materials imaging and characterization as well as heat transfer applications.[1,2] One of the most fascinating results of recent theoretical work is the prediction of significantly enhanced photon tunneling in the near-field range as compared to the blackbody limit.[3,4] A key feature for the enhancement is the quasi-monochromatic spectrum when the systems support surface phonon-polaritons[5,6] or surface plasmon-polaritons.[7,8] Being able to control radiative transfer at the nanoscale is of utmost importance in developing ultrafast spectroscopy for all-optical characterization of molecular and nanoscaled systems,[9] photovoltaic solar cells,[10] and temperature control in nanostructures.[11,12]

Radiative thermal transfer between large objects has been considered mostly when fundamental understanding and novel applications are put forward. These include two half-spaces,[5] spheres, approximated as single dipoles,[4] or a sphere and a half space.[13,14] The analysis is usually done in the framework of fluctuation electrodynamics introduced by Rytov et al.[15] This formalism has been used to predict that evanescent waves have the leading contribution in the near-field regime at separations less than 10 μm.[3] Experiments have also demonstrated this effect.[6,16,17] Measurements of radiative cooling of nanostructures have not only shown the existence of near-field enhancement but also utilized it for cooling.[12]

Recently, it was shown that graphene, an atomically thin layer of C atoms arranged in a honeycomb lattice, can also be used for near-field radiation enhancement.[18−20] This is a consequence of the temperature-dependent localized to the graphene surface plasmons with very long decay times. Besides the planar graphene, quasi-one-dimensional nanoribbons or confined in all directions graphene nanostructures, such as nanodisks or flakes of other forms[21,22] have also shown interesting plasmon properties. Doping and external electric fields combined with quantization effects provide new channels of tuning.[23]

The microscopic nature of near-field radiation between nanostructures materials in terms of specific atoms and their characteristics is a relatively less studied problem. Most theoretical descriptions are performed under the assumption that the entire nanostructured objects behave essentially as effective dipoles at different temperatures.[24] However, at separations at the nanoscale, this approximation is not valid. The particular atomic structure becomes relevant, and the radiation process has to be described as a result of the electromagnetic interaction involving the many atoms and their collective contributions.[25] Investigating the atomistic composition and its influence on the near-field radiation is of particular importance to graphitic structures to provide novel ways for nanoscaled heat transfer control.[26]

Electromagnetic transport between nanostructures is challenging, not only due to the need to take into account the
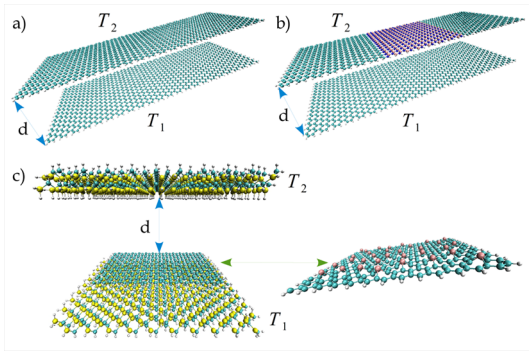
Figure 1. (a) Two identical GNS flakes; (b) hybrid BN-GNS and a GNS flakes; (c) a NS-SiC substrate and a GNR covered NS-SiC substrate; (d) a GNS with randomly distributed Al substitutional atoms. The SiC surface bonds are saturated either by H or Cl atoms. The top and bottom structures separated by d are held at temperatures T_1 and T_2.

discrete atomic structure, but also due to the nontrivial boundary conditions. Often such systems contain several types of species, and since the number of atoms is finite, each type can transmit electromagnetic heat very differently. Depending on the location of the atoms and their quantity, the heat exchange at the nanoscale maybe very different. Thus previous approaches utilizing macroscopic electrodynamics[18−20,27] with response properties derived from mean-field theories are not appropriate. Here, we present a microscopic study using a model that takes into account the atomic structure of the objects. The formulation uses the coupled dipole method (CDM) supplemented by the fluctuation dissipation theorem. Our focus is on finite graphene nanostructures, for which we present a comprehensive picture of radiative heat exchange by taking into account the collective nature of this process and nontrivial boundary conditions.

Within this model, the interacting objects are represented as arrangements of a finite number of dipoles positioned at the location of each atom. The atoms are described as fluctuating dipoles using the dissipative Drude−Lorentz model[28,29]

$$\alpha_i(\omega) = \frac{\alpha_{0,i}\omega_{0,i}^2}{\omega_{0,i}^2 - \omega^2 - i\gamma_{0,i}\omega} \tag{1}$$

where $\alpha_{0,i}$ is the static atomic polarizability, $\gamma_{0,i}$ is the damping parameter, $\omega_{0,i}$ is the characteristic frequency for the ith atom in each nanostructure.

The radiative power Φ_{12} dissipated in object 1 due to object 2 from the work of the electromagnetic field is found via $\Phi_{12} = 2Re[\Sigma_{i,j=1}^{N_1,N_2}\langle -i\omega \mathbf{p}_i^{ind}(\omega)\cdot\mathbf{E}_i(\mathbf{r}_j)\rangle]$, where $i = 1,...N_1$, $j = 1,...N_2$ denote the atomic dipoles in object 1 with N_1 atoms and object 2 with N_2 atoms, respectively.[30] $\mathbf{p}_i^{ind}$ is the induced dipole moment at site $\mathbf{r}_i$ due to the field at that site $\mathbf{E}_i(\mathbf{r}_j)$ from the dipole located at $\mathbf{r}_j$. Applying the fluctuation dissipation theorem,[24] the exchanged power is found as

$$\Phi = \Phi_{12} - \Phi_{21}$$
$$= 3\int_0^\infty \frac{d\omega}{2\pi}[\Theta(\omega, T_1) - \Theta(\omega, T_2)]T(\omega) \tag{2}$$

$$T(\omega) = \sum_{i=1;j=1}^{N_1,N_2} \tau_{ij}(\omega) \tag{3}$$

where $\Theta(\omega,T_{1,2}) = \hbar\omega /(e^{\hbar\omega/k_B T_{1,2}} - 1)$, with $T_{1,2}$ being the temperatures of each object.

The transmission coefficient $T(\omega)$ is a key property quantifying the heat exchange between the objects. It accounts for the microscopic nature of the exchange process and it includes the optical characteristics of each atom. It can be found via the near-field radiation for dipolar systems[24,31] $\tau_{ij} = 4\omega^4 \mathrm{Im}(a_i)\mathrm{Im}(a_j)\mathrm{Tr}[\Gamma_{ij}^\dagger(\omega)\Gamma_{ij}(\omega)]/(3c^4)$. The Green's function dyadic $\Gamma_{ij}(\omega)$ with ij components captures the propagation of the electromagnetic field due to the presence of the objects comprised of finite number of dipoles N_1,N_2, and it relates the electric field at site $\mathbf{r}_j$ to the fluctuating dipoles $\mathbf{p}_j^{fl}$

$$\mathbf{E}_i(\mathbf{r}_j) = \omega^2\mu_0\Gamma_{ij}(\omega)p_j^{fl} \tag{4}$$

The Green's function dyadic is then calculated using the CDM first proposed in ref 32. According to this approach, the electric field can also be expressed as

$$\mathbf{E}_i(\mathbf{r}_j) = \mu_0\omega^2\Gamma_{ij}^0\mathbf{p}_j^{fl} + \frac{\omega^2}{c^2}\sum_{l=1}^{N_1+N_2}\Gamma_{il}^0\alpha_l\mathbf{E}_l(\mathbf{r}_j) \tag{5}$$

where Γ_{ij}^0 are the components of the free electromagnetic dyadic $\Gamma_{ij}^0 = [\exp(ikR_{ij})/4\pi R_{ij}][(1 + ikR_{ij} - 1/k^2R_{ij}^2) \times 1 + [(3 - 3ikR_{ij} - k^2R_{ij}^2)/k^2R_{ij}^2]\hat{\mathbf{R}}_{ij} \otimes \hat{\mathbf{R}}_{ij}]$. Also, $\mathbf{R}_{ij}$ is the displacement vector connecting the dipoles at sites i,j, $|\mathbf{R}_{ij}|$ is its magnitude, and $\hat{\mathbf{R}}_{ij}$ is the unit vector. One obtains coupled $3(N_1 + N_2)$ equations, which can be solved self-consistently yielding

$$\Gamma_{ij}^0 = \frac{\omega^4}{c^4}\Gamma_{ij}\sum_{k=1}^{N_1+N_2}(\delta_{ik}\delta_{kj} - \sum_{l=1}^{N_1+N_2}\Gamma_{ik}^0\alpha_k\Gamma_{kl}^0\alpha_l) \tag{6}$$

The above expression can now be used to find the components of Γ_{ij} utilizing standard matrix operations.

The CDM is a powerful technique when dealing especially with long-ranged electromagnetic interactions, such as van der Waals forces between systems with finite number of atoms.[28,29] It takes into account the discrete atomic nature of the interacting objects together with all many-body interactions. Recently, the interest toward this approach has been renewed as researchers have utilized it in existing density functional theory codes to calculate van der Waals forces self-consistently at a reasonable computational cost.[33]

Here we show that out-of-thermal equilibrium phenomena, such as near-field radiation exchange, can also benefit from the advantages that the CDM offers for nanostructures. Calculating the Green's function self-consistently takes into account the collective nature of the electromagnetic radiation by the inclusion of all many-body contributions. The temperature of each atom is captured through the fluctuation−dissipation theorem. In this way, nontrivial boundary conditions of nanostructures can be dealt with, and heat exchange can be calculated involving even more than two finite objects.

The first system we consider are two graphene nanostructures (GNSs) of a rectangular form held at two different temperatures. In one case, both flakes are the same (Figure 1a) and in the other case, one of the structures is a hybrid formation of a h-BN patch positioned in the center (BN-GNS) (Figure 1b). All edges are saturated by H atoms. Hybrid structures have been shown to possess distinct from pure graphene or h-BN layers electronic and thermal properties.[34,35] Here we study how the electromagnetic radiation of such hybrid systems is affected.

4197

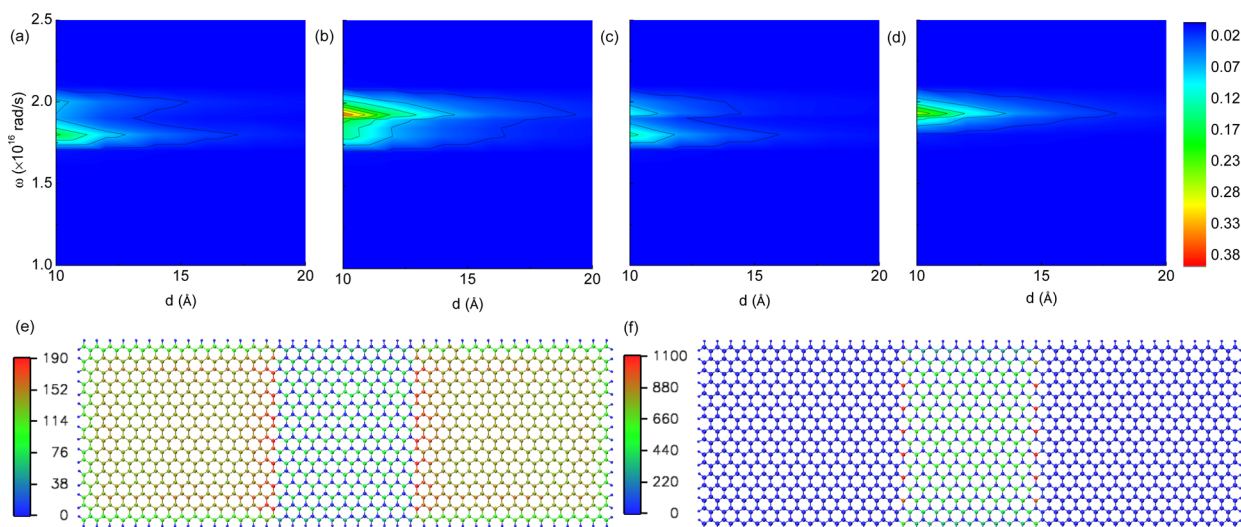dx.doi.org/10.1021/jz402337f | J. Phys. Chem. Lett. 2013, 4, 4196−4200

Figure 2. Frequency vs separation contour plots of total transmission coefficient $t(\omega)$ for (a) two GNSs, (b) a BN-GNS and a GNS. Contour plots of transmission coefficient of all (c) C atoms; (d) all B atoms of the BN-GNS to the second GNS. Atomically resolved transmission coefficients ($\times 10^{-6}$) of the BN-GNS at (e) $\omega = 1.8 \times 10^{16}$ rad/s; (f) $\omega = 2 \times 10^{16}$ rad/s for $d = 10$ Å^3. Atomic characteristics: $\alpha_{0,H} = 0.25$ Å^3, $\omega_{0,H} = 1.41 \times 10^{16}$ rad/s, $\alpha_{0,C} = 0.85$ Å^3, $\omega_{0,C} = 1.85 \times 10^{16}$ rad/s, $\alpha_{0,B} = 1.282$ Å^3, $\omega_{0,B} = 1.91 \times 10^{16}$ rad/s, $\alpha_{0,N} = 0.914$ Å^3, $\omega_{0,N} = 2.68 \times 10^{16}$ rad/s. The damping parameters are $\gamma_{0,i} = 0.05\omega_{0,i}$ for all atoms.

The transmission coefficient $T(\omega)$ is calculated using eqs 3−6) for two GNSs and BN-GNS/GNS (Figure 1. The dimensions of the identical structures are a 10 nm ×3.5 nm (2820 atoms in total). Ab initio results are used for the characteristics frequencies $\omega_{i,0}$ and static polarizabilities $\alpha_{i,0}$ for the different atoms.[28,36−38] Figure 2a,b show the contour plots of $T(\omega)$ for ω as the object separation is varied. It is seen that $T(\omega)$ for the two GNSs is localized asymmetrically around $\omega \sim 1.8 \times 10^{16}$ and it decays as two peaks as d increases. $T(\omega)$ for the hybrid system is much more symmetric around $\omega \sim 1.91 \times 10^{16}$ rad/s as it decays as one peak. It is evident that the transmission coefficient is stronger for the system involving the BN hybrid structure.

We can calculate not only the total transmission coefficient, but also the transmission coefficient between particular atoms or groups of atoms simply by specifying the desired summation in eq 3. In Figure 2c,d, we show the contour plots for the coefficient for all C atoms (summation for i in eq 3 is over only all C atoms of the BN-GNS, while $j = 1 - N_2$) and for all B atoms (summation for i in eq 3 is over only all B atoms of the BN-GNS, while $j = 1 - N_2$). Results for the N and H atoms are not shown, as their contribution is very small. One sees that the presence of B atoms has a relatively strong effect on $T(\omega)$. The B atoms are the reason for the enhanced transmission coefficient and one-peak structure for the BN-GNS/GNS as compared to the one for the two GNSs.

Figure 2e,f shows the transmission coefficient for each atom i of the BN-GNS flake to the GNS, which means that one sums over the atoms of the GNS $\sum_{j=1}^{N_2} \tau_{ij} (\omega)$ only according to eq 3. The atomically resolved T is not uniform. Depending on ω, particular atoms will transmit more electromagnetic energy as compared to the others. Clearly, C atoms will transmit the most when $\omega \sim \omega_{0,C}$ (Figure 2c), while the B atoms have the highest coefficient when $\omega \sim \omega_{0,B}$ (Figure 2d). The H and N atoms are relatively inactive. Our calculations show that in addition to the particular characteristic frequency, the static polarizabilities are also an important factor. We find that the primary reason for the larger magnitude of the B transmission coefficient at $\omega \geq \omega_{0,B}$ as compared to the one for C is due to the fact that $\alpha_{0,B} > $

$\alpha_{0,C}$. Even at $\omega = \omega_{0,N}$, $\omega_{0,H}$, the transmission coefficient for N and H atoms is much smaller due to their small static polarizabilities.

We also investigate the near-field heat transfer between a nanostructured SiC (NS-SiC) substrate and another one with a GNS on top; Figure 3c). Each NS-SiC contains two layers, and its dimensions are 4.5 nm ×4.5 nm ×0.59 nm (1279 atoms in total). Growing graphene on a SiC substrate is currently an active research area due to potential applications for electronics.[39] Researchers have developed various methods to achieve epitaxial graphene layers on top of SiC. Intercalation by atoms, such as H, Cl, F, Au, Ge, etc.., aid the separation of the graphene as the surface bonds of the substrate are saturated.[39,40] Graphene layers with doping or under external electric fields on top of SiC have also been studied for electronics applications.[41] Furthermore, SiC is an optically active material with surface phonon polaritons being able to strongly interact with graphene surface plasmons. As a result, near-field radiation enhancement is possible as the graphene properties are modified upon doping or external fields.[15,16]

Our focus is on the specific role of the SiC surface saturation bonds and doped GNS by metallic impurities. Both factors are currently being pursued as possible routes to tailor graphene electronic and magnetic properties. Here, we investigate how the near-field radiation of GNS-based systems is affected by the NS-SiC substrate morphology and metallic doping of the graphene flake from a microscopic point of view.

The NS-SiC is taken to have surface bonds saturated by H or Cl. The GNS/NS-SiC separation of 3 Å corresponds to the equilibrium distance from our ab initio simulations. In Figure 3a,b, we show the contour plot of ω vs d for the total transmission coefficient between the top substrate and the GNS/NS-SiC with H and Cl bonds, respectively. It is found that $T(\omega)$ is localized around $\omega_{0,Si}$ for H saturated SiC. A second peak is found around $\omega_{0,C}$, which is very weak ($T = 0.02$ at $d = 10$ Å) and it is not shown. Because of the relatively small C static polarizability, the transmission is dominated entirely by the Si atoms. Once the H is substituted by Cl, the transmission coefficient acquires a second peak localized around $\omega_{0,Cl}$
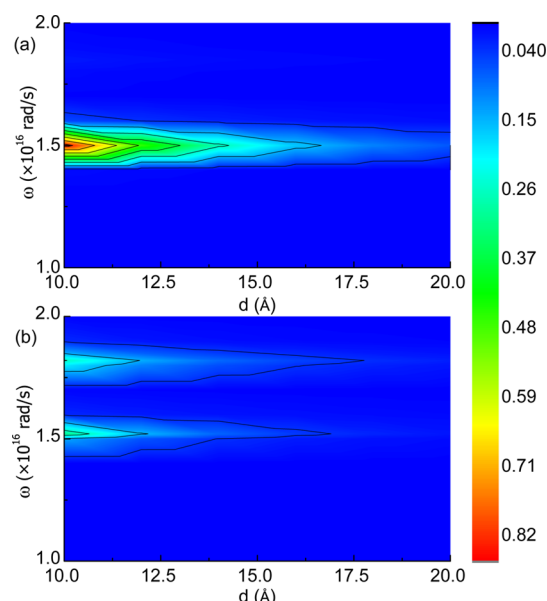
Figure 3. Contour plots of ω vs d for the total transmission coefficient between a NS-SiC and GNS/NS-SiC for (a) H-saturated and (b) Cl-saturated SiC surface bonds. Atomic characteristics: $\alpha_{0,Si} = 3.71$ Å^3, $\omega_{0,Si} = 1.52 \times 10^{16}$ rad/s, $\alpha_{0,Cl} = 2.38$ Å^3, $\omega_{0,Cl} = 1.82 \times 10^{16}$ rad/s. Also, $\gamma_{0,i} = 0.05\omega_{0,i}$ for all atoms. The rest of the parameters are the same as in Figure 2.

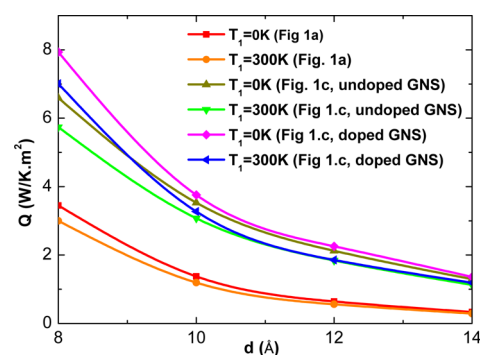**Figure 4.** The exchanged heat power per unit area as a function of separation between the nanostructures. The top system is held at $T_2 = 500$ K.

reducing the strength of the one associated with the Si atoms at $\omega_{0,Si}$. This is attributed to the large static Cl polarizability.

We also consider a doped GNS with Al atoms substituting 8% of the C atoms; Figure 1d). Our ab initio simulations show that the metallic atom forms strong covalent bonds with the C network and it is accompanied by a local curvature due to the large Al−C bond relative to the C−C bond in agreement with previous studies.[42] The total transmission coefficient between the top substrate and the doped GNS/SiC is calculated using eqs 3 (SiC surface bonds are saturated by Cl). The result is very similar to Figure 3b; however, an additional peak centered around $\omega_{0,Al}$ appears (not shown). This relatively weak peak ($T = 0.04$ at $d = 10$ Å) can be enhanced if the doping concentration of the GNS is increased.

Finally, we calculate the radiative heat power per unit area using eq 2 for different GNS settings. The shown results in Figure 4 indicate that Q is the smallest between two GNSs. Also, the radiative power exchanged between the top SiC and the bottom GNS(undoped)/SiC is not affected significantly by the graphene flake. Q practically stays the same regardless of the presence of the flake. This is consistent with the very small contribution of the GNS to the total transmission coefficient relative to the Cl saturated SiC.

Metallic doping changes this picture. Although the concentration is only 8%, its role in Q is much more significant. It is realized that the heat exchange is determined by $T(\omega)$, $\Theta(\omega,T)$, and their overlap according to eq 2. $\Theta(\omega,T)$ is most significant when ω is in the low-frequency regime for the studied temperatures, and it quickly decays for larger ω since $\hbar\omega/k_BT$ increases. Thus it is desirable that $T(\omega)$ has contributions in the low frequency range. This is precisely the role of the Al doping in the GNS sandwiched between the NS-SiC substrates as our analysis for the transmission coefficient has shown. As a result, Q is enhanced by ∼22%

for doped graphene flake as compared to the undoped one. Consequently, larger doping results in larger heat power.

In summary, we have investigated near-field radiation for graphene nanostructures using a coupled dipole method suitable for out-of-thermal equilibrium phenomena. This is a microscopic approach capable of taking into account the atomic structure and nontrivial geometry explicitly, while previous studies[15,16] have utilized macroscopic electrodynamics. We consider the radiative process involving two graphene structures and a graphene structure between two nano-structured SiC substrates at nanometer separations and show how hybrid systems, substrate bond saturation, and doping via metallic impurities affect the near-field radiation. The comprehensive understanding of how the GNS doping determines the heat exchange enhancement at the nanoscale is especially useful. In general, one can explore the relation between the transmission coefficient and the temperature function $\Theta(\omega,T)$ to devise ways to control the heat power atomistically even when more than two systems are involved.

■ **AUTHOR INFORMATION**

Corresponding Authors
*E-mail: anhphan@mail.usf.edu.
*E-mail: lmwoods@usf.edu.

■ **REFERENCES**

(1) Alvarez-Puebla, R.; Liz-Marzan, L. M.; de Abajo, F. J. G. *J. Phys. Chem. Lett.* **2010**, *1*, 2428−2434.
(2) Jones, A. C.; Raschke, M. B. *Nano Lett.* **2012**, *12*, 1475−1481.
(3) Polder, D.; Hove, M. V. *Phys. Rev. B* **1971**, *4*, 3303−3314.
(4) Volokitin, A. I.; Persson, B. N. J. *Rev. Mod. Phys.* **2007**, *79*, 1291−1329.
(5) Joulain, K.; Mulet, J. P.; Marquier, F.; Carminati, R.; Greffet, J. J. *Surf. Sci. Rep.* **2005**, *57*−59112.
(6) Shen, S.; Narayanaswamy, A.; Chen, G. *Nano Lett.* **2009**, *9*, 2909−2913.
(7) Basu, S.; Lee, B. J.; Zhang, Z. M. *J. Heat Transfer* **2010**, *132*, 023302.
(8) Passian, A.; Lereu, A. L.; Arakawa, E. T.; Wig, A.; Thundat, T.; Ferrell, T. L. *Opt. Lett.* **2005**, *30*, 41−43.

(9) Berweger, S.; Atkin, J. M.; Olmon, R. L.; Raschke, M. B. *J. Phys. Chem. Lett.* **2012**, *3*, 945−952.

(10) Hagglund, C.; Apell, S. P. *J. Phys. Chem. Lett.* **2012**, *3*, 1275−1285.

(11) Yannopapas, V.; Vitanov, N. V. *Phys. Rev. Lett.* **2013**, *110*, 044302.

(12) Guha, B.; Otey, C.; Poitras, C. B.; Fan, S.; Lipson, M. *Nano Lett.* **2012**, *12*, 4546−4550.

(13) Narayanaswamy, A.; Shen, S.; Chen, G. *Phys. Rev. B* **2008**, *78*, 115303−115306.

(14) Krueger, M.; Emig, T.; Kardar, M. *Phys. Rev. Lett.* **2011**, *106*, 210404−210407.

(15) Rytov, S. M.; Kravtsov, Y. A.; Tatarskii, V. I. *Principles of Statistical Radiophysics 4: Wave Propagation Through Random Media*; Springer-Verlag: Berlin, 1989.

(16) Kittel, A.; Muller-Hirsch, W.; Parisi, J.; Biehs, S.-A.; Reddig, D.; Holthaus, M. *Phys. Rev. Lett.* **2005**, *95*, 224301.

(17) Kralik, T.; Hanzelka, P.; Zobac, M.; Musilova, V.; Fort, T.; Horak, M. *Phys. Rev. Lett.* **2012**, *109*, 224302.

(18) Svetovoy, V. B.; Zwol, P. J. V.; Chevrier, J. *Phys. Rev. B* **2012**, *85*, 155418.

(19) Ilic, O.; Jablan, M.; Joannopoulos, J. D.; Celanovic, I.; Buljan, H.; Soljacic, M. *Phys. Rev. B* **2012**, *85*, 155422.

(20) Messina, R.; Ben-Abdallah, P. *Sci. Rep.* **2013**, *3*, 1383.

(21) Cong, C. X.; Yu, T.; Ni, Z. H.; Liu, L.; Shen, Z. X.; Huang, W. *J. Phys. Chem. C* **2009**, *113*, 6529.

(22) Park, K. H.; Kim, B. H.; Song, S. H.; Kwon, J.; Kong, B. S.; Kang, K.; Jeon, S. *Nano Lett.* **2012**, *12*, 2871−2876.

(23) Thongrattanasiri, S.; Koppens, F. H. L.; Abajo, F. J. G. D. *Phys. Rev. Lett.* **2012**, *108*, 047401.

(24) Ben-Abdallah, P.; Biehs, S.-A.; Joulain, K. *Phys. Rev. Lett.* **2011**, *107*, 114301.

(25) Forster, T. *Ann. Phys.* **1948**, *2*, 55−75.

(26) Nemilentsau, A. M.; Rotkin, S. V. *ACS Nano* **2012**, *6*, 4298−4304.

(27) Zwol, P. J. V.; Thiele, S.; Berger, C.; Heer, W. A. D.; Chevrier, J. *Phys. Rev. Lett.* **2012**, *109*, 264301.

(28) Shtogun, Y. V.; Woods, L. M. *J. Phys. Chem. Lett.* **2010**, *1* (9), 1356−1362.

(29) Cole, M. W.; Velegol, D.; Kim, H.-Y.; Kucas, A. A. *Mol. Simul.* **2009**, *35*, 849−866.

(30) Jackson, J. D. *Classical Electrodynamics*; Wiley: Hoboken, NJ, 1999).

(31) Volokitin, A. I.; Persson, B. N. *J. Phys. Rev. B* **2001**, *63*, 205404.

(32) Purcell, E. M.; Pennypacker, C. R. *Astrophys. J.* **1973**, *186*, 705−714.

(33) Tkatchenko, A.; DiStasio, R. A., Jr.; Car, R.; Scheffler, M. *Phys. Rev. Lett.* **2012**, *108*, 236402.

(34) Lam, K.-T.; Lu, Y.; Feng, Y. P.; Liang, G. *Appl. Phys. Lett.* **2011**, *98*, 022101.

(35) Jiang, J.-W.; Wang, J.-S.; Wang, B.-S. *Appl. Phys. Lett.* **2011**, *99*, 043109.

(36) Jensen, L.; Astrand, P.-O.; Sylvester-Hvid, K. O.; Mikkelsen, K. V. *J. Phys. Chem. A* **2000**, *104* (7), 1563−1569.

(37) Kongsted, J.; Osted, A.; Jensen, L.; Astrand, P.-O.; Mikkelsen, K. V. *J. Phys. Chem. B* **2001**, *105* (42), 10243−10248.

(38) Chu, X.; Dalgarno, A. *J. Chem. Phys.* **2004**, *121*, 4083.

(39) Cheng, Y. C.; Zhu, Z. Y.; Schwingenschlogl, U. *Europhys. Lett.* **2013**, *101*, 27008.

(40) Hsu, C.-H.; Lin, W.-H.; Ozolins, V.; Chuang, F.-C. *Appl. Phys. Lett.* **2012**, *100*, 063115.

(41) Zhu, Y.; Murali, S.; Cai, W.; Li, X.; Suk, J. W.; Potts, J. R.; Ruoff, R. S. *Adv. Mater.* **2010**, *22* (35), 3906−24.

(42) Dai, J.; Yuan, J. *Phys. Rev. B* **2010**, *81*, 165414.